Dipolar fermions in a multilayer geometry

M. Callegari,[1,2] M. M. Parish,[3,4,*] and F. M. Marchetti[2,†]

[1]*Department of Physics and Astronomy "Galileo Galilei", University of Padova, Via Marzolo 8, 35131 Padova, Italy*

[2]*Departamento de Física Teórica de la Materia Condensada & Condensed Matter Physics Center (IFIMAC), Universidad Autónoma de Madrid, Madrid 28049, Spain*

[3]*London Centre for Nanotechnology, Gordon Street, London WC1H 0AH, United Kingdom*

[4]*School of Physics & Astronomy, Monash University, Victoria 3800, Australia*

(Received 26 January 2016; revised manuscript received 31 January 2017; published 21 February 2017)

We investigate the behavior of identical dipolar fermions with aligned dipole moments in two-dimensional multilayers at zero temperature. We consider density instabilities that are driven by the attractive part of the dipolar interaction and, for the case of bilayers, we elucidate the properties of the stripe phase recently predicted to exist in this interaction regime. When the number of layers is increased, we find that this "attractive" stripe phase exists for an increasingly larger range of dipole angles, and if the interlayer distance is sufficiently small, the stripe phase eventually spans the full range of angles, including the situation where the dipole moments are aligned perpendicular to the planes. However, in this regime, we expect the behavior to be strongly modified by the binding of dipoles between layers. In the limit of an infinite number of layers, we derive an analytic expression for the mean-field interlayer effects in the density-density response function and, using this result, we find that the stripe phase is replaced by a collapse of the dipolar system.

DOI: 10.1103/PhysRevB.95.085124

I. INTRODUCTION

Motivated by the prospect of novel many-body phases generated by anisotropic long-range dipolar interactions, much attention has recently been devoted to ultracold polar molecules and magnetic atoms [1–3]. Dipolar fermions, in particular, can be used to simulate strongly correlated phenomena in electron systems, including charge density modulations (stripes) and unconventional superconductivity [4–6].

Quantum degeneracy has already been achieved for dipolar Fermi gases of atoms with a permanent magnetic dipole moment such as chromium [7], dysprosium [8], and erbium [9]. This has enabled the observation of dipole-driven Fermi surface deformations in the Fermi liquid phase [10]. However, to investigate many-body phenomena at stronger dipole-dipole interactions, it appears necessary to use polar molecules, which generally possess larger dipole moments—the electric dipole moment can be as large as 5.5 Debye in the case of ^{133}Cs ^{6}Li [11]. Thus far, there has been major progress towards producing quantum degenerate clouds of long-lived fermionic dipolar molecules using ^{40}K ^{87}Rb [12–14], ^{23}Na ^{6}Li [15], ^{133}Cs ^{6}Li [16], and ^{23}Na ^{40}K [17,18].

The dipole-dipole interaction can be further tuned and enhanced by confining the polar molecules to *two-dimensional* (2D) layers. Such a geometry has been used to suppress chemical reactions [19] and to stabilize the gas against mechanical collapse, which arises in three dimensions for a sufficiently strong interaction [20–26]. Furthermore, by aligning all the dipole moments with a strong electric field, the nature of the effective 2D dipolar interaction within the plane may be externally manipulated: The dipole-dipole repulsion is maximized by aligning the dipole moments perpendicular to the plane, while anisotropy and attraction are gradually introduced by varying the dipole tilt (see Fig. 1). This possibility has stimulated much theoretical work on dipolar fermionic gases in single and multilayer 2D geometries [3].

For the single-layer geometry and for small (but nonzero) tilting angles, the weakly interacting system corresponds to a Landau Fermi liquid with deformed Fermi surface [27], similarly to the case in 3D. With increasing dipolar interaction (or cloud density), the system is then predicted to undergo a transition to a unidirectional density modulated phase [28–31], where the modulations are perpendicular to the direction of the dipole tilt. Such a "stripe" phase has also been shown to exist in the *isotropic* case where the dipoles are aligned perpendicular to the layer, thus requiring the system to spontaneously break the rotational symmetry [32]. This result has recently been supported by density functional theory calculations [33], which predict a transition to a stripe phase followed by a transition to a triangular Wigner crystal at higher coupling. Quantum Monte Carlo calculations also find a Wigner crystal phase for the case of perpendicularly aligned dipoles, although at a much higher dipolar interaction than that obtained from density functional theory [34].

For tilting angles greater than a critical angle, the attractive part of the dipolar interaction can lead to p-wave superfluidity in the single-layer system [35], and this phase may even coexist with stripe order [36]. A sufficiently strong attraction eventually drives a mechanical instability of the cloud towards collapse [28,31,32,35,37]. However, interestingly, if one instead considers a bilayer geometry, the additional layer stabilizes the collapse at large tilt angles—as long as the dipoles are aligned out of the plane ($\theta < \pi/2$)—to form a new stripe phase, where the density modulations are oriented along the direction of the dipole tilt [38].

In this paper, we investigate such a stripe phase, which is generated by the attractive part of the dipolar interaction for large enough dipole tilt angle. We start by elucidating its properties in the case of the bilayer, where we provide a new

*meera.parish@monash.edu

†francesca.marchetti@uam.es

 ©2017 American Physical Society

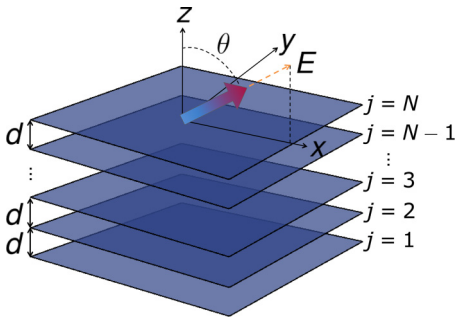

FIG. 1. Schematic representation of the system geometry. A gas of dipolar fermions is confined to N 2D layers labeled by an index $j = 1,2,\ldots,N$ and separated by a distance d. We assume that each layer has the same density of dipoles n. The dipole moment of each fermion is aligned by an electric field $\mathbf{E} = (E_x,0,E_z)$ in the x-z plane ($\varphi = 0$ direction), at an angle θ with respect to the $\hat{\mathbf{z}}$ direction.

classical argument for how the stripes in each layer are shifted with respect to each other. Then we extend our results for the density-density response function to the multilayer geometry. We employ an approach based on a version of the Singwi-Tosi-Land-Sjölander (STLS) scheme [32,38,39] that incorporates exchange interactions only, which should be reasonable for the "attractive" stripe phase [38], provided that the interlayer binding of dipoles [40–42] is weak. Note, however, that we neglect the possibility of other stripe phases driven by the strong intralayer repulsion [38,43].

As the number of layers N is increased, we find that the attractive stripe phase spans an increasingly larger region of the phase diagram. However, this stripe phase eventually gives way to collapse in the $N \to \infty$ limit.

The paper is organized as follows: In Sec. II, we describe the system geometry and introduce the STLS scheme which allows us to evaluate the density-density response function matrix in the multilayer geometry; in Sec. III, we describe the properties of the density instabilities driven by the attractive part of the interlayer dipolar interaction and, in Sec. III A, we explain via a classical model how the stripes in each layer are shifted with respect to each other. In Sec. IV, we extend the results to a generic number of layers N, while in Sec. V we consider the $N \to \infty$ limit. In Sec. VI we assess the influence of interlayer correlations on the predicted stripe phase by estimating the bound state properties in a bilayer (i.e., dimer in Sec. VI A), as well as for an infinite number of layers (i.e., semiclassical bound chain in Sec. VI B). The concluding remarks are gathered in Sec. VII.

II. MULTILAYER SYSTEM AND MODEL

We consider a gas of polar fermionic molecules in a multilayer geometry, as shown in the schematic picture in Fig. 1. The molecules have a dipole moment D and are confined to N two-dimensional layers, each labeled by an index $j = 1,2,\ldots,N$ and equally separated by a distance d. We assume that the dipoles are aligned by an external electric field $\mathbf{E} = (E_x,0,E_z)$ in the x-z plane, which is tilted at an angle θ with respect to the $\hat{\mathbf{z}}$ direction. Within each layer, we parametrize the x-y in-plane wave vector by polar coordinates $\mathbf{q} = (q,\varphi)$, where $\varphi = 0$ corresponds to the direction of the dipole tilt.

In the limit $qW \ll 1$, where W is the layer width, the effective 2D intralayer interaction between dipoles takes the following form [44]:

$$v_{jj}(\mathbf{q}) \equiv v(\mathbf{q}) = V_0 - 2\pi D^2 q \xi(\theta,\varphi), \tag{1}$$

where $\xi(\theta,\varphi) = \cos^2\theta - \sin^2\theta\cos^2\varphi$. Here, $\mathbf{q}$ corresponds to the relative wave vector between two dipoles. The constant V_0 is a short-range contact interaction term that in general depends on the width W [44], yielding a natural UV cutoff. Since we are considering identical fermions, the system properties will not depend on V_0. The 2D dipolar interaction can alternatively be regularized by considering physical electrical dipoles with a finite size l, which, like W, act as a UV cutoff [45]. In this case, for $ql \ll 1$, the intralayer interaction recovers the same expression (1).

In the limit where the layer width is much smaller than the layer separation, $W \ll d$, the interaction between two dipoles in different layers $j > l$ is given by [46]:

$$v_{jl}(\mathbf{q}) = -2\pi D^2 q e^{-(j-l)qd}[\xi(\theta,\varphi) + i\sin 2\theta\cos\varphi]. \tag{2}$$

The remaining interlayer interactions can be obtained from the condition $v_{lj}(\mathbf{q}) = v_{jl}(-\mathbf{q}) = v_{jl}^*(\mathbf{q})$, which is derived from the fact that the dipolar interaction is always real in real space. Likewise, the momentum-space interaction is complex for $\theta \neq 0$ since the real-space interaction is not invariant under the transformation $\mathbf{r} \mapsto -\mathbf{r}$.

Assuming that each layer has the same density n, we define the Fermi wave vector $k_F = \sqrt{4\pi n}$. This allows us to define the dimensionless interaction strength $U = mD^2k_F$, where m is the fermion mass (henceforth we fix $\hbar = 1$). The other parameters that can be independently varied are the dipole tilt angle θ and the dimensionless layer separation $k_F d$.

Response function and STLS equations

Similarly to Ref. [38], we make use of linear response theory to analyze density wave instabilities. In the multilayer system, the linear density response δn to an external perturbing potential V^{ext} defines the density-density response function matrix [47],

$$\delta n_j(\mathbf{q},\omega) = \sum_l \chi_{jl}(\mathbf{q},\omega) V_l^{\text{ext}}(\mathbf{q},\omega), \tag{3}$$

where j,l are the layer indices. A divergence in the static density-density response function matrix $\chi_{jl}(\mathbf{q},\omega = 0)$ signals an instability of the system. Specifically, the system is unstable towards forming a stripe phase when the smallest eigenvalue $\tilde{\chi}_{\min}(\mathbf{q})$ of the static response function matrix first diverges at a critical value of the wave vector $\mathbf{q}_c = (q_c,\varphi_c)$.

While the response function is known exactly for the non-interacting gas, typically one can only incorporate the effect of interactions approximately. A standard approach is the random phase approximation (RPA), where one replaces the external potential with one that contains an effective potential due to the perturbed density: $V_j^{\text{ext}} \mapsto V_j^{\text{ext}} + \sum_l v_{jl}\delta n_l$. However, RPA neglects exchange correlations, which are always important in the dipolar system, even in the long-wavelength limit $q \to 0$ [32]. This issue may be remedied using a conserving

Hartree-Fock approximation [30,31,43], but we choose a simpler and physically motivated approach where correlations are included via local field factors $G_{jl}(\mathbf{q})$ [48]. This yields the inverse density-density response function matrix

$$\hat{\chi}^{-1}{}_{jl}(\mathbf{q},\omega) = \frac{\delta_{jl}}{\Pi(\mathbf{q},\omega)} - v_{jl}(\mathbf{q})[1 - G_{jl}(\mathbf{q})], \tag{4}$$

where $\Pi(\mathbf{q},\omega)$ is the noninteracting response function, which, for equal density layers, reads as [47,49]

$$\Pi(\mathbf{q},i\omega) = \frac{m}{2\pi b}\{\sqrt{2}[a + \sqrt{a^2 + (\omega b)^2}]^{1/2} - b\},$$

with $a = \frac{b^2}{4} - b\frac{k_F^2}{m} - \omega^2$ and $b = \frac{q^2}{m}$. RPA corresponds to taking the limit where the layer-resolved local field factors $G_{jl}(\mathbf{q})$ in Eq. (4) are all zero.

The response function (4) can be related to the layer-resolved static structure factor $S_{jl}(\mathbf{q})$ by the fluctuation-dissipation theorem:

$$S_{jl}(\mathbf{q}) = -\frac{1}{\pi n}\int_0^\infty d\omega \chi_{jl}(\mathbf{q},i\omega). \tag{5}$$

In the noninteracting limit, the static structure factor is diagonal, i.e., $S^{(0)}_{jl}(\mathbf{q}) = \delta_{jl}\ S^{(0)}(q)$, and can be evaluated exactly (see Appendix), where

$$S^{(0)}(q) = \frac{2}{\pi}\arcsin\left(\frac{q}{2k_F}\right) + \frac{q}{\pi k_F}\sqrt{1 - \left(\frac{q}{2k_F}\right)^2}, \tag{6}$$

for $q \leqslant 2k_F$, while $S^{(0)}(q) = 1$ for $q > 2k_F$ [47,48].

To determine the local field factors, we consider the STLS approximation scheme, where we have the expression [39,47]:

$$G_{jl}(\mathbf{q}) = \frac{1}{n}\int \frac{d\mathbf{k}}{(2\pi)^2}\frac{\mathbf{q}\cdot\mathbf{k}}{q^2}\frac{v_{jl}(\mathbf{k})}{v_{jj}(\mathbf{q})}[\delta_{jl} - S_{jl}(\mathbf{q}-\mathbf{k})]. \tag{7}$$

This approach ensures that all particle-particle correlations present in the system, as encapsulated in the structure factor, are fed back into the local field factor. The approximate relation (7) is derived using a classical analogy—see, e.g., Appendix 10 in Ref. [48]. In principle, $G_{jl}(\mathbf{q})$ can be determined self-consistently by solving Eqs. (4), (5), and (7). Note that this self-consistent approach includes correlations beyond RPA and is not just limited to exchange correlations. As such, the STLS scheme has proven to be a powerful method for treating strongly correlated electron systems such as the 2D electron gas [48]. We previously adapted an improved version of this scheme to the dipolar system, both in the single- [32] and double-layer [38] geometries. The scheme is improved by imposing, at each iteration step, the condition that the intralayer pair correlation function is zero at zero distance, $g_{jj}(0) = 0$, where,

$$g_{jl}(\mathbf{r}) = 1 + \frac{1}{n}\int \frac{d\mathbf{q}}{(2\pi)^2}e^{i\mathbf{q}\cdot\mathbf{r}}[S_{jl}(\mathbf{q}) - \delta_{jl}]. \tag{8}$$

This ensures that the intralayer static structure factor $S_{jj}(\mathbf{q})$ is dominated by Pauli exclusion in the short wavelength limit, $q \gg 2k_F$, and that the system response is independent of the short-range contact interaction term V_0 and the cutoff W.

In the following, we first review the bilayer case and describe the instability to a stripe phase occurring for large tilt angles θ, where the modulations are oriented along the dipole tilt, i.e., along $\varphi = 0$. We then show how the instability to the $\varphi = 0$ stripe phase can be well described using exchange correlations only, and we use this to investigate its existence in the multilayer geometry.

III. THE $\varphi = 0$ STRIPE PHASE IN BILAYERS

The case of two layers ($N = 2$) was previously analyzed within the STLS self-consistent approximation scheme in Ref. [38]. Here, at sufficiently small tilt angles $\theta < \theta_c$, and by increasing the value of the dimensionless coupling strength U, there is an instability from the uniform phase to a stripe phase with modulations along the y axis ($\varphi = \pi/2$ stripe phase). The instability to this stripe phase is driven by intralayer correlations beyond exchange, which are induced by the repulsive part of the intralayer interaction potential $v(\mathbf{q})$. By contrast, for $\theta_c < \theta < \pi/2$, the system develops an instability to a stripe phase along the x axis ($\varphi = 0$ stripe phase). While for a single layer, the attractive sliver of the intralayer interaction produces a collapse of the dipolar Fermi gas at large tilt angles, the bilayer geometry stabilizes the collapse in favor of a $\varphi = 0$ stripe phase, which thus derives from a competition between the intralayer attraction in the $\varphi = 0$ direction and the interlayer interaction.

Interestingly, this latter stripe phase can be accurately described using intralayer exchange correlations only. In fact, it was found for this phase that the intralayer pair correlation function $g_{jj}(\mathbf{r})$ deviated only slightly from the noninteracting case, while the interlayer correlation function $g_{12}(\mathbf{r}) \sim 1$. In terms of local correlations, the interlayer local field factor can thus be neglected, $G_{12}(\mathbf{r}) = 0$, while the intralayer one $G_{jj}(\mathbf{q}) \equiv G(\mathbf{q})$ is determined from the noninteracting intralayer structure factor (6):

$$G(\mathbf{q}) = \frac{1}{n}\int \frac{d\mathbf{k}}{(2\pi)^2}\frac{\mathbf{q}\cdot\mathbf{k}}{q^2}\frac{v(\mathbf{k})}{v(\mathbf{q})}[1 - S^{(0)}(q)]. \tag{9}$$

We refer to this approximation scheme as the exchange-only STLS approximation (X-STLS). For the single-layer case [32], this approach yielded an instability towards collapse at large θ that agreed with the predictions from Hartree-Fock calculations [28,30,31,35].

The phase boundary between the normal phase and the $\varphi = 0$ stripe phase obtained from the full STLS scheme is displayed in Fig. 2 ([green] open triangles) and is compared with the results of the X-STLS approximation ([blue] solid line). The value of the critical tilt angle for such a phase is $\theta_c \simeq 0.75$ if evaluated within the full STLS scheme, while it is slightly higher, $\theta_c \simeq 0.79$, if evaluated within the X-STLS approximation. It turns out that, for the phase boundary, the X-STLS approximation works particularly well at large angles, all the way up to $\theta = \pi/2$, where, for $U \gtrsim 1.57$ ([red] diamond symbol and thick solid line), the gas collapses because the Fermi pressure is not high enough to counteract the strong dipolar attraction.

The eigenvectors of the density-density response function (4) determine the phase-shift η between layers, and for the bilayer geometry we have found that [38]:

$$e^{i\eta} = -\frac{v_{12}(\mathbf{q})[1 - G_{12}(\mathbf{q})]}{|v_{12}(\mathbf{q})[1 - G_{12}(\mathbf{q})]|}. \tag{10}$$

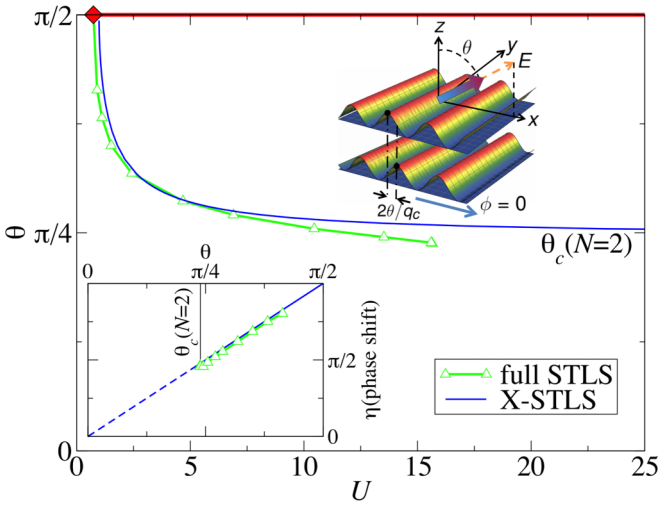

FIG. 2. Main panel: Phase boundary for the $\varphi = 0$ stripe phase in the two-layer geometry as a function of the tilt angle θ and the dimensionless interaction strength U at fixed interlayer distance $k_F d = 2$. Density modulations are in the direction $\varphi = 0$ of the dipole tilt (schematic figure). The instability to this phase is to the right of the plotted boundaries: The full STLS results [38] ([green] open triangles) are compared to the results obtained with exchange-only correlations ([blue] solid line), also referred to as the X-STLS approximation scheme. Within X-STLS, the $\varphi = 0$ stripe phase appears for $\theta > \theta_c \simeq 0.79$. At $\theta = \pi/2$, the gas is unstable towards mechanical collapse for $U \gtrsim 1.57$ ([red] diamond symbol and thick solid line), where the gas compressibility is infinite. The density modulations in the two layers have a phase shift η (lower inset) equal to 2θ, i.e., the shift between the modulations $2\theta/q_c$ (schematic figure).

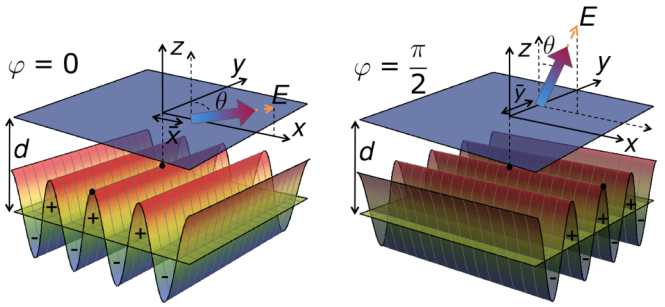

FIG. 3. Schematic representation of a single dipole in the top layer interacting classically with an infinite bottom layer of dipoles arranged in a stripe modulated phase. As in Fig. 1, all dipoles are aligned by an electric field **E**. In the left (right) panel, the single dipole is shifted by $\bar{x}$ ($\bar{y}$) with respect to one of the stripe crests for the $\varphi = 0$ ($\varphi = \frac{\pi}{2}$) stripe phase.

For both $\varphi = \pi/2$ and $\varphi = 0$ stripe phases, we find that the interlayer phase shift between the modulations is independent of the dipole interaction strength U and the layer distance d. In particular, for the $\varphi = \pi/2$ stripe phase, both the interaction and the local field factor are real and thus both layer modulations are always in phase, i.e., $\eta = 0$. On the other hand, for the $\varphi = 0$ stripe phase, if we consider an exchange-only approximation (X-STLS) for which $G_{12}(\mathbf{q}) = 0$, we obtain a phase shift of $\eta = 2\theta$. The phase shift for the $\varphi = 0$ stripe phase is plotted in the inset of Fig. 2. We see a very good agreement between the full STLS results ([green] open triangles) and the simplified X-STLS scheme ([blue] solid line). The $\varphi = 0$ result may at first appear counterintuitive, but it can be reproduced by evaluating the classical interaction energy between an infinite layer of dipoles in one layer and a single dipole in the second layer, as we discuss next.

Classical model

For the bilayer geometry, a simple classical model can easily explain the phase shifts found in both $\varphi = 0$ and $\varphi = \pi/2$ stripe phases. Let us consider the simplified case of an infinite layer of dipoles whose density is modulated sinusoidally with a wave vector $q_c = 2\pi/\lambda_c$ and amplitude ρ_0. We further assume that this interacts classically with a single dipole positioned at $\mathbf{r}_0$ in the other layer. The two layer densities are thus, respectively, given by:

$$\rho^{(1)}(\mathbf{r}) = n + \rho_0 \cos(\mathbf{q}_c \cdot \mathbf{r}) \tag{11}$$

$$\rho^{(2)}(\mathbf{r}') = \delta(\mathbf{r}' - \mathbf{r}_0). \tag{12}$$

For the $\varphi = 0$ ($\varphi = \pi/2$) stripe phase we have $\hat{\mathbf{q}}_c = \hat{\mathbf{x}}$ ($\hat{\mathbf{q}}_c = \hat{\mathbf{y}}$) and $\mathbf{r}_0 = (\bar{x}, 0)$ ($\mathbf{r}_0 = (0, \bar{y})$)—see the schematic representation of both geometries in Fig. 3. The classical interaction energy is given by

$$E_{\rm cl} = \int d\mathbf{r} d\mathbf{r}' \rho^{(1)}(\mathbf{r}) v_{12}(\mathbf{r} - \mathbf{r}') \rho^{(2)}(\mathbf{r}'), \tag{13}$$

where

$$v_{12}(\mathbf{r}) = D^2 \frac{x^2 + y^2 + d^2 - 3(x \sin\theta + d\cos\theta)^2}{(x^2 + y^2 + d^2)^{5/2}}$$

is the interlayer potential (assuming that the distance d is much larger than the layer thickness W). For a uniform density distribution $\rho^{(1)}(\mathbf{r}) = n$, the classical interaction energy would be zero; therefore only deviations from the average density in $\rho^{(1)}(\mathbf{r})$ contribute (either positively or negatively) to $E_{\rm cl}$.

Considering the Fourier transforms $\rho^{(1,2)}(\mathbf{r}) = \int \frac{d\mathbf{q}}{(2\pi)^2} \rho^{(1,2)}(\mathbf{q}) e^{i\mathbf{q}\cdot\mathbf{r}}$ and $v_{12}(\mathbf{r}) = \int \frac{d\mathbf{q}}{(2\pi)^2} v_{12}(\mathbf{q}) e^{i\mathbf{q}\cdot\mathbf{r}}$, we can rewrite (13) to obtain

$$E_{\rm cl} = \int \frac{d\mathbf{q}}{(2\pi)^2} \rho^{(1)}(-\mathbf{q}) v_{12}(\mathbf{q}) \rho^{(2)}(\mathbf{q}), \tag{14}$$

where

$$\rho^{(1)}(\mathbf{q}) = (2\pi)^2 \left[n\delta(\mathbf{q}) + \rho_0 \frac{\delta(\mathbf{q} + \mathbf{q}_c) + \delta(\mathbf{q} - \mathbf{q}_c)}{2} \right]$$

$$\rho^{(2)}(\mathbf{q}) = e^{-i\mathbf{q}\cdot\mathbf{r}_0}.$$

Thus, as $v_{12}(0) = 0$, we get in general

$$E_{\rm cl} = \frac{\rho_0}{2} [v_{12}(-\mathbf{q}_c) e^{i\mathbf{q}_c\cdot\mathbf{r}_0} + v_{12}(\mathbf{q}_c) e^{-i\mathbf{q}_c\cdot\mathbf{r}_0}], \tag{15}$$

and specifically for the two stripe phases:

$$E_{\rm cl}^{\varphi=0} = -\frac{4\pi^2 D^2 \rho_0}{\lambda_c} e^{-2\pi d/\lambda_c} \cos\left(2\pi \frac{\bar{x}}{\lambda_c} - 2\theta\right)$$

$$E_{\rm cl}^{\varphi=\pi/2} = -\frac{4\pi^2 D^2 \rho_0}{\lambda_c} e^{-2\pi d/\lambda_c} \cos^2\theta \cos\left(2\pi \frac{\bar{y}}{\lambda_c}\right).$$

Therefore, we can conclude that, for both stripe configurations, the distance, $\bar{x}$ or $\bar{y}$, that minimizes the interaction energy $E_{\rm cl}$ does not depend on the dipole strength D or the layer separation d. Further, for the $\varphi = \pi/2$ stripe phase, the best configuration is the one where the single dipole in layer 2 aligns with the maximum density of layer 1, i.e., $\bar{y}_{\rm min} = 0$. By contrast, for the $\varphi = 0$ stripe phase, the optimal configuration is for a phase shift equal to twice the dipole tilt angle θ, i.e., $2\pi\bar{x}_{\rm min}/\lambda_c = 2\theta$. An analogous calculation was carried out for the $\varphi = \pi/2$ stripe phase in the simplified limit where the density modulations were approximated as discrete dipolar wires [43].

We now wish to extend these results to multiple layer $N > 2$ configurations. We have seen that the presence of a second layer stabilizes the region of collapse at large tilt angles $\theta_c < \theta < \pi/2$, replacing it with a novel stripe phase oriented along $\varphi = 0$ [38]. Furthermore, within the X-STLS approximation, the critical tilt angle for the $\varphi = 0$ stripe phase in bilayers is $\theta_c(N = 2) \sim 0.79$, which is lower than that for collapse in the single layer, $\theta_c(N = 1) \sim 0.89$. It is therefore natural to ask whether the $\varphi = 0$ stripe phase will tend to dominate the phase diagram as the number of layers N is increased.

IV. N LAYERS

Motivated by the results obtained for the bilayer system, we now apply the X-STLS approximation scheme to the general case of finite $N > 2$ layers and evaluate the occurrence of the $\varphi = 0$ stripe phase when varying the system parameters. In particular, by neglecting all correlations except for the exchange ones, we assume that all off-diagonal local field factors are zero, $G_{j\neq l}(\mathbf{q}) = 0$, while the intralayer ones $G(\mathbf{q})$ are evaluated according to Eq. (9). To locate the stripe instabilities, we extract the smallest eigenvalue of the static density-density response function matrix, $\tilde{\chi}_{\rm min}(\mathbf{q})$, and determine the critical wave vector $\mathbf{q}_c = (q_c,\varphi_c)$ at which it first diverges. If the instability is for a specific angle φ_c, then it signals the formation of a density wave with modulations in that direction and with a period set by q_c. Here, we always find that $\varphi_c = 0$, as in the bilayer case.

At the stripe transition, the phase shifts η_{jl} between the stripes in different layers j,l are extracted from the eigenvector associated with the smallest eigenvalue, $\tilde{\chi}_{\rm min}(\mathbf{q}_c)$. We find that the behavior of the multilayer system is a natural extension of the bilayer case: The phase shift between nearest neighbor layers $\eta_{j,j+1}$ grows monotonically with the tilt angle θ, although linearly only for small values of θ. Moreover, the phase shift between more distant layers is always proportional to $\eta_{j,j+1}$.

To gain insight into the phase diagram of the multilayer system, we first focus on the trilayer, $N = 3$. In Fig. 4, we plot the phase boundaries for the instability to a $\varphi = 0$ stripe phase (left panel) and the associated critical wave vectors q_c/k_F (right panel) for different values of the layer distance dk_F. The qualitative behavior we observe here is common to any number of layers N, including the case of a bilayer $N = 2$. For large enough layer distance d, the $\varphi = 0$ stripe phase can only occur for values of the tilt angle greater than a critical angle θ_c, i.e., at the stripe instability boundary, we have $U \to \infty$ for $\theta \to \theta_c$ ([green] circle symbols). However, when the layer distance decreases, we find that θ_c eventually reaches zero at a critical distance d_c ([violet] star symbols): Here, the $\varphi = 0$ stripe phase spans the entire range of tilt angles θ. For smaller distances, $d < d_c$, stripe formation is always possible for sufficiently large but finite values of the interaction strength U, even for dipoles aligned perpendicular to the planes.

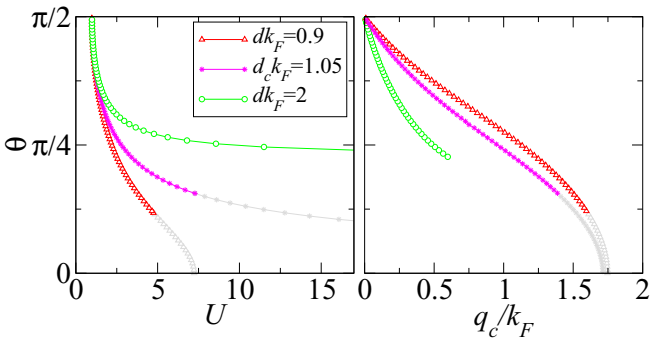

FIG. 4. Evolution of the $\varphi = 0$ stripe phase for the trilayer $N = 3$ geometry when varying the dimensionless layer separation dk_F. Left panel: phase boundary in the θ versus U plane; the instability to the stripe phase is on the right side of the plotted boundary. The boundary is gray at higher values of U and smaller values of the tilt angle θ, where interlayer pairing correlations cannot be neglected (see Sec. VI A). Right panel: Rescaled stripe wave vector q_c/k_F at the phase boundaries as a function of the tilt angle θ.

Note that when decreasing the value of dk_F, eventually our exchange-only formalism becomes questionable, since it neglects interlayer correlations. In particular, for $k_F d \lesssim 1$ and for sufficiently small θ, interlayer pairing (e.g., dimers in the two-layer configuration [50] and bound chains in multilayers [42,51]) is expected to dominate over stripe formation, and this is not included in the X-STLS approximation scheme. However, even though small θ_c may be unphysical, the critical distance d_c still provides a useful measure of the system's behavior, since it constrains the overall shape of the stripe phase boundary in the U-θ plane. In Sec. VI, we estimate the region of the phase diagram where interlayer correlations cannot be neglected.

We next investigate whether the $\varphi = 0$ stripe phase can dominate the phase diagram as the number of layers N is increased. To this end, we plot in Fig. 5 the phase boundaries (left panels) for the $\varphi = 0$ stripe phase for different values of N. We observe qualitatively different behavior depending on whether the distance d is above or below $\sim 1.47/k_F$, corresponding to the critical distance d_c for $N \to \infty$, as derived in Sec. V. When $d > d_c(N \to \infty)$ (lower panels of Fig. 5), the $\varphi = 0$ stripe phase exists for an increasingly larger range of dipole tilt angles as N increases, but the critical angle θ_c finally saturates to a finite positive value. When instead $d < d_c(N \to \infty)$ (upper panels of Fig. 5), the stripe phase eventually spans the full range of angles, including the situation where the dipole moments are aligned perpendicular to the planes.

These results are summarized in Fig. 6, where we plot, as a function of $1/N$, the critical value of the interlayer distance $d_c k_F$ at which the $\varphi = 0$ stripe phase first spans the full range of dipole tilt angles. The data for $N \to \infty$ in the figures

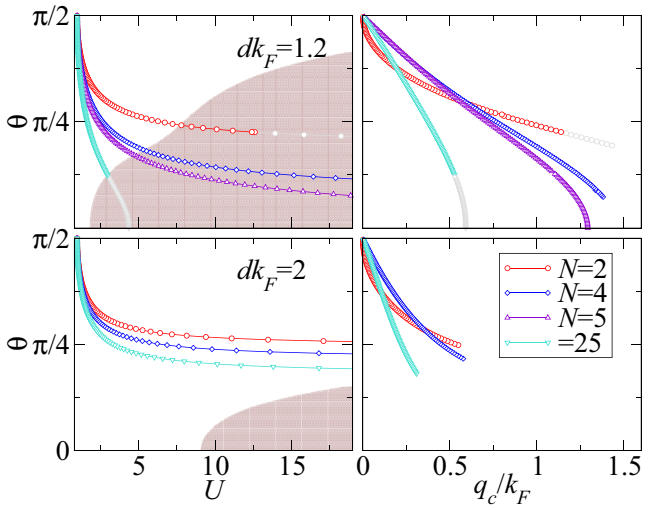

FIG. 5. Phase boundaries (left panels) and rescaled stripe wave vector at the boundaries q_c/k_F (right panels) for the $\varphi = 0$ stripe phase for different values of the number of layers N and two fixed values of the layer distance: $dk_F = 1.2$ (top panels) and $dk_F = 2$ (bottom panels). The phase boundary for stripe formation at $N = 2$ ([red] open circles) is gray when the system preferentially forms dimers. The shaded region indicates the crossover to a "bound-state regime" dominated by dipolar chains (here evaluated for the case of an infinite number of layers).

are evaluated following the procedure explained in the next section.

V. THE $N \to \infty$ LIMIT

We now show how the calculation for the $\varphi = 0$ stripe instability can be extended to the limit of an infinite number of layers. The key point is that the interlayer interaction potential $v_{jl}(\mathbf{q})$ only depends on the layer index difference $|j - l|$, so that, for a system with periodic boundary conditions and $N \gg 1$, we can make a transformation from the layer index

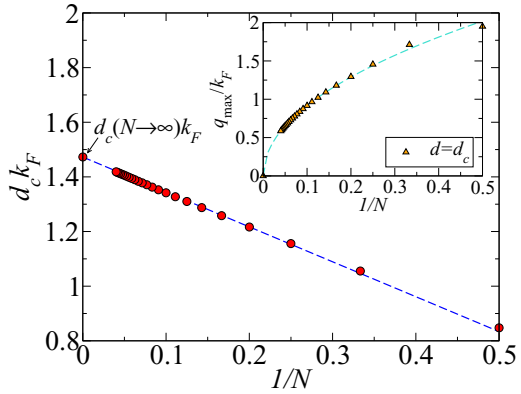

FIG. 6. Critical value of the interlayer distance $d_c k_F$ at which $\theta_c = 0$ (at $U \to \infty$) as a function of the inverse number of layers, $1/N$. In the limit $N \to \infty$, $d_c k_F = 1.47$. Numerical data are represented as (red) circles, while the dashed (blue) line is a linear fit to the data. Inset: maximum value of the stripe wave vector q_c/k_F for $d = d_c$ as a function of $1/N$. Data are (orange) triangles, while the (turquoise) dashed line is a nonlinear fit giving $f(1/N) = 2.83(1/N)^{0.49}$.

space $j = 1,2,\ldots,N$ to the reciprocal space $p = 2\pi m/N$, where $m = -N/2,\ldots,N/2$ [52]:

$$\tilde{u}_p = \sum_{j-l=-N}^{N} e^{-i(j-l)p} v_{jl}. \tag{16}$$

Of course, in the actual system, we do not have periodic boundary conditions, but this should not change the physics in the limit $N \to \infty$. Inserting Eq. (2) yields the analytical solution

$$\tilde{u}_p(\mathbf{q}) = -2\pi D^2 q \left[\frac{\zeta(\theta,\varphi)}{e^{ip+qd} - 1} + \frac{\zeta(\theta,\varphi+\pi)}{e^{-ip+qd} - 1} \right], \tag{17}$$

where $\zeta(\theta,\varphi) = \xi(\theta,\varphi) + i \sin 2\theta \cos\varphi$, and where we have taken the limit $N \to \infty$ after evaluating the geometric series.

We thus obtain the following expression for the eigenvalues of the inverse density-density response function:

$$\tilde{\chi}_p^{-1}(\mathbf{q},\omega) = \frac{1}{\Pi(\mathbf{q},\omega)} - v(\mathbf{q})[1 - G(\mathbf{q})] - \tilde{u}_p(\mathbf{q}). \tag{18}$$

To investigate the instabilities, we take the static limit, $\omega = 0$, and determine the values of p and $\mathbf{q}$ for which $\tilde{\chi}_p^{-1}$ first hits zero. In practice, this means we must find the value of p that maximizes $-\tilde{u}_p(\mathbf{q})$ for each $\mathbf{q}$. Solving for the stationary points gives us two solutions:

$$p_{i=1,2} = 2 \arctan \left[\frac{(e^{qd} \mp 1) \sin\theta \cos\varphi}{(e^{qd} \pm 1) \cos\theta} \right] + \pi \delta_{i,2}, \tag{19}$$

where the argument is positive if we assume $0 \leqslant \varphi \leqslant \pi/2$. The first solution p_1 corresponds to the maximum of $-\tilde{u}_p(\mathbf{q})$, where we have

$$\tilde{u}_{p_1}(\mathbf{q}) = -4\pi D^2 q \left(\frac{\cos^2\theta}{e^{qd} - 1} - \frac{\cos^2\varphi \sin^2\theta}{e^{qd} + 1} \right). \tag{20}$$

Thus we have now considerably simplified the problem, as we only have to find the zero of the maximum inverse eigenvalue of the static response, $\tilde{\chi}_{p_1}^{-1}(\mathbf{q},0)$, as a function of $\mathbf{q}$.

In this limit, we always find that $(q_c,\varphi_c) = 0$, i.e., by increasing the number of layers to infinity, the gas becomes unstable towards mechanical collapse. Here, the gas compressibility, which is proportional to the static response function at $\mathbf{q} = 0$, is infinite. The results for the phase boundary of such a collapsed phase are summarized in Fig. 7 and are qualitatively similar to the boundaries found for the $\varphi = 0$ stripe phase in the case of a finite number of layers. Below the critical layer distance $d_c k_F \simeq 1.47$, the collapsed phase exists for any value of the dipole tilt angle, including $\theta = 0$. As discussed in the next section, interlayer binding cannot be neglected for small tilt angles in this limit. However, the value of d_c still determines the behavior of the phase boundary at larger θ, as shown in Fig. 7.

The behavior of the infinite N multilayer system is reminiscent of that expected for the 3D dipolar Fermi gas, where one also has collapse for sufficiently large dipolar interactions [21]. In particular, the $\theta = 0$ case possesses the same rotational symmetry as the 3D gas with aligned dipole moments. Therefore, it is instructive to compare the onset of collapse for $\theta = 0$ in the multilayer system to that in the 3D case. First, one can define a 3D density for the multilayer

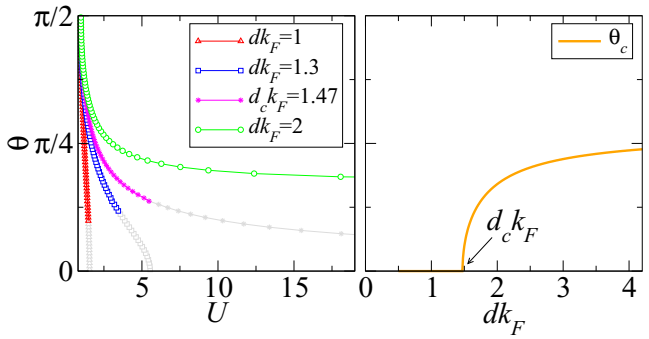

FIG. 7. Left panel: Phase boundary of the collapsed region for an infinite number of layers $N \to \infty$ and different values of the rescaled layer density dk_F. The instability to collapse is signalled by an infinite compressibility of the dipolar gas, i.e., by a divergence of the static response function for $\mathbf{q}_c = 0$. While for $d > d_c$, collapse occurs only for a tilt angle larger than a critical value θ_c, for $d < d_c$, the collapsed phase spans the entire range of angles. The phase boundaries are plotted in gray when the system crosses over to the "bound state regime" dominated by infinitely long dipolar chains (see Sec. VI B). Right panel: We plot the asymptotic values of the tilt angle at the phase boundary for $U \to \infty$, θ_c, as a function of the rescaled layer distance dk_F; we find that the critical distance for infinite layers is given by $d_c(N \to \infty)k_F = 1.47$.

geometry:

$$n_{3D} = \frac{n}{d} = \frac{k_F^3}{4\pi(k_F d)}. \tag{21}$$

This then yields the corresponding 3D dimensionless interaction parameter:

$$U_{3D} \equiv mD^2 n_{3D}^{1/3} = \frac{U}{(4\pi k_F d)^{1/3}}. \tag{22}$$

In the 3D dipolar gas, the collapse instability occurs at $U_{3D} \simeq 2.4$ [21]. Thus, to obtain a comparable U_{3D} for collapse in the multilayer system, we require $dk_F \simeq 1.31$ and $U \simeq 6.12$. In our 2D infinite layer configuration, we can interpret the parameter dk_F as an effective Fermi surface "deformation" parameter if we treat $2\pi/d$ as a Fermi momentum in the z direction. This assumes that it is the interparticle spacing rather than the fermion exchange that is the key feature of the Fermi surface deformation in 3D when considering the collapse instability. For the multilayer geometry, the ratio between the Fermi momenta in the z and radial directions is then given by $2\pi/(k_F d)$, thus yielding $k_{F,z}/k_{F,r} \sim 4.8$ at the collapse instability. This is not so dissimilar from that obtained for the 3D Fermi gas within Hartree-Fock mean-field theory, where $k_{F,z}/k_{F,r} \sim 2$ [21]. In the layered system, we can effectively tune the deformation such that the critical U_{3D} for collapse is raised (lowered) by increasing (decreasing) dk_F. Eventually, when $d > d_c$, the Fermi surface is not sufficiently elongated along the dipole direction to produce collapse.

VI. BOUND STATES IN MULTILAYERS

Thus far, we have neglected strong interlayer correlations, which are expected to dominate in the multilayer system for small d. While we have restricted our calculations to $k_F d \gtrsim 1$, there is still the possibility of interlayer bound states (e.g., chains) when U is sufficiently large [42]. Therefore, in this section, we estimate the importance of interlayer correlations by solving for the interlayer bound states in the simplified limit of one dipole in each layer, and then comparing the bound-state in-plane size with the interparticle spacing within each layer: If the bound state is comparatively large within the 2D planes, then the interlayer correlations are negligible and we expect our X-STLS approximation scheme to be reasonable. Due to the complexity of the multiparticle bound state problem, we focus on two limiting cases: (i) the dimer in the bilayer, which may be determined exactly, and (ii) the chain in an infinite number of layers, where we will use a semiclassical approximation.

A. Dimer in the bilayer

For the case of the bilayer with one dipole in each layer, we must solve the following equation to obtain the dimer bound state:

$$E\psi(\mathbf{k}) = 2\epsilon_{\mathbf{k}}\psi(\mathbf{k}) + \sum_{\mathbf{k}'} v_{21}(\mathbf{k}-\mathbf{k}')\psi(\mathbf{k}'), \tag{23}$$

where $\psi(\mathbf{k})$ is the momentum-space wave function for the two dipoles in relative coordinates, E is the dimer energy and $\epsilon_{\mathbf{k}} = \mathbf{k}^2/2m$ the dipole kinetic energy. Note that the center-of-mass momentum is decoupled from the relative motion and can thus be set to zero.

A dimer bound state exists for all angles θ and interaction strengths $U_d = mD^2/d$ [50]. We estimate the dimer size k_0 in momentum space by equating it to the point at which $|\psi(\mathbf{k})|^2$ is half its maximum value, i.e., we define $|\psi(k_0, \varphi = 0)|^2 = \frac{1}{2}|\psi(\mathbf{0})|^2$, where we have taken the direction ($\varphi = 0$) along which the dimer is most tightly bound.

We plot in the left panel of Fig. 8 the rescaled dimer size in momentum space, $k_0 d$, as a function of the interaction strength U_d for two different angles. In the limit $k_0/k_F \gg 1$, the dimer state is tightly bound and the many-body bilayer system corresponds to a gas of bosonic dimers. On the other hand, interlayer correlations are weak in the opposite limit $k_0/k_F \ll 1$. Thus, $k_0/k_F \gtrsim 1$ approximately defines the region of parameter space (which we denote as the "bound-state regime"), where interlayer pairing correlations cannot be

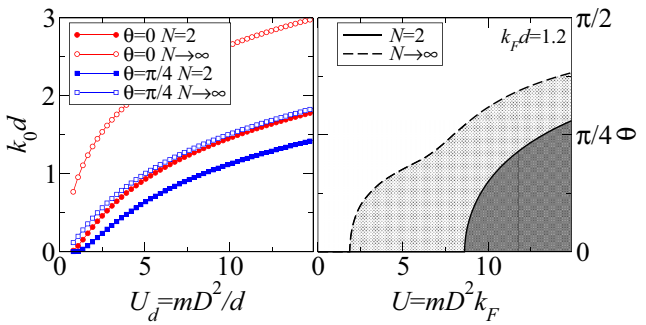

FIG. 8. Left panel: Size in momentum space, $k_0 d$, of dimers ($N = 2$ [filled symbols]) and bound chains ($N \to \infty$ [empty symbols]) as a function of the interaction strength U_d for $\theta = 0$ ([red] circles) and $\theta = \pi/4$ ([blue] squares). Right panel: "bound-state" region for fixed $k_F d = 1.2$, indicating where $k_0/k_F \gtrsim 1$ and interlayer correlations are important (see Fig. 5).

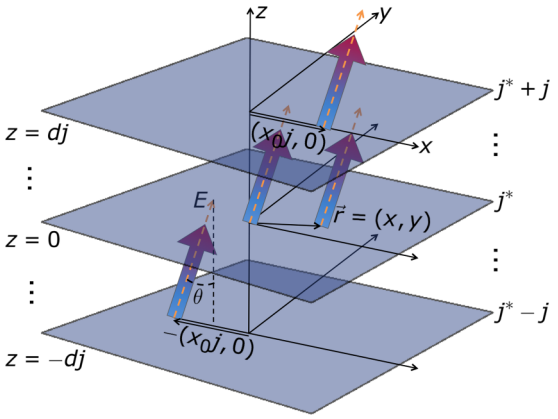

FIG. 9. Classical configuration of an infinite chain of static dipoles (dipole in the layer j^* positioned at $\mathbf{r} = 0$): dipoles in adjacent top and bottom layers are shifted by a vector $\pm\mathbf{r}_{01} = \pm(x_0,0)$, respectively, in order to minimize the potential energy $v_{\rm cl}(x_0)$ (see text). Fluctuations around this classical configuration are introduced by allowing one dipole, say in layer j^*, to move freely to any in-plane position $\mathbf{r}$.

ignored. This crossover region is plotted in the right panel of Fig. 8 ($k_F d = 1.2$): Here, the X-STLS results are likely to be inaccurate. For this reason, in Figs. 4 and 5, we have grayed out the parts of the stripe boundaries that lie within the bound-state regime.

B. Bound chain in the limit $N \to \infty$

For multiple layers with one dipole per layer, the problem quickly becomes intractable for large N. Therefore, to proceed further, we consider the limit $N \to \infty$ and apply a semiclassical approximation: First we approximate the chain as classical, where the kinetic energy of the dipoles is neglected and the system simply minimizes the potential energy; then we estimate the size of the fluctuations around this state by allowing one of the dipoles to be mobile while keeping all the remaining dipoles fixed.

A classical infinite chain of static dipoles for a generic tilt angle θ is expected to arrange such that dipoles in adjacent top and bottom layers are shifted by a vector $\pm\mathbf{r}_{01} = \pm(x_0,0)$, respectively (see schematic Fig. 9). This configuration minimizes the potential energy felt by one dipole due to all the other dipoles:

$$v_{\rm cl}(x_0) = \frac{2\zeta(3)D^2}{\left(x_0^2+d^2\right)^{3/2}}\left[1 - 3\frac{(x_0\sin\theta + d\cos\theta)^2}{x_0^2+d^2}\right],$$

with Riemann zeta function $\zeta(3) = \sum_{j=1}^{\infty} j^{-3} \simeq 1.202$. While a classical chain of dipoles arranges vertically when $\theta = 0$, for a finite tilt angle, the chain slope x_0/d minimizing the classical potential $v_{\rm cl}(x_0)$ is an increasing function of θ, and approximately $x_0/d \sim \tan(\theta/2)$ at small angles.

We now allow one single dipole, say in the layer j^*, to fluctuate and move freely to any position $\mathbf{r}$ (see Fig. 9). In real space, the effective potential felt by the dipole in the j^*th layer due to all the other dipoles is given by

$$\tilde{v}_{\rm eff}(\mathbf{r}) = \sum_{j=2}^{\infty}\left[v_{j1}^{\theta}(\mathbf{r}-\mathbf{r}_{0j}) + v_{j1}^{\pi-\theta}(\mathbf{r}+\mathbf{r}_{0j})\right],$$

where $\mathbf{r}_{0j} = (x_0 j, 0)$, $v_{ij}^{\theta}(\mathbf{r}) = v_{ji}^{\theta}(-\mathbf{r})$, and:

$$v_{1j}^{\theta}(\mathbf{r}) = D^2\frac{x^2+y^2+(dj)^2 - 3(x\sin\theta + dj\cos\theta)^2}{[x^2+y^2+(dj)^2]^{5/2}}.$$

Clearly, we have $\tilde{v}_{\rm eff}(\mathbf{r}=0) = v_{\rm cl}(x_0)$. By considering the Fourier transform of $\tilde{v}_{\rm eff}(\mathbf{r})$, we obtain the following equation for the momentum-space wave function of the mobile dipole in layer j^*:

$$E\psi_\infty(\mathbf{k}) = \epsilon_{\mathbf{k}}\psi_\infty(\mathbf{k}) + \sum_{\mathbf{k}'} v_{\rm eff}(\mathbf{k}-\mathbf{k}')\psi_\infty(\mathbf{k}'), \qquad (24)$$

where the effective potential it experiences is

$$v_{\rm eff}(\mathbf{q}) = 2\sum_{j=2}^{\infty}{\rm Re}[e^{iqx_0(j-1)\cos\varphi}v_{j1}(\mathbf{q})]$$
$$= -4\pi D^2 q\,{\rm Re}\left[\frac{\xi(\theta,\varphi) + i\sin 2\theta\cos\varphi}{e^{q(d-ix_0\cos\varphi)}-1}\right].$$

In this case, we define $|\psi_\infty(k_0,\varphi=\pi/2)|^2 = \frac{1}{2}|\psi_\infty(\mathbf{0})|^2$. Note that, in contrast to the bilayer case, the direction where the chain bound state is most tightly bound (i.e., has the largest k_0) is $\varphi = \pi/2$. This is because the anisotropy of the static dipole chain creates a shallower potential along the $\varphi = 0$ direction. We expect our semiclassical approach to provide an upper bound on k_0, since we have suppressed the kinetic energy of all the other dipoles. Thus, it will likely overestimate the size of the bound-state region in the phase diagram.

Like for the dimer case, we plot in the left panel of Fig. 8 the rescaled bound-state size $k_0 d$ as a function of the interaction strength U_d. We find that long chains have a larger binding energy per dipole and are more strongly bound than dimers, in agreement with Ref. [42]. As a consequence, the crossover boundary to the "bound-state regime" for a given tilt angle θ occurs at smaller values of the interaction strength U for $N \to \infty$ than for $N = 2$ (right panel of Fig. 8). We thus conclude that the behavior at small tilt angles is likely to be dominated by the creation of dipolar bound chains rather than stripe formation (see shaded region top left panel of Fig. 5 where $k_F d = 1.2$). This circumstance is avoided when $k_F d$ is sufficiently large, as shown in Fig. 7 and in the bottom panels of Fig. 5 at $k_F d = 2$.

VII. CONCLUDING REMARKS

In this work, we have analyzed the density instabilities of dipolar Fermi multilayer systems that are driven by the attractive part of the dipolar interaction. We have argued that such instabilities are dominated by exchange correlations and can thus be described using a simplified exchange-only STLS approach, provided that the interlayer correlations are sufficiently weak. We find that the attraction-driven $\varphi = 0$ stripe phase expands to fill the phase diagram with an increasing number of layers N. However, at the same time, the stripe wave vector decreases so that the stripe phase is eventually replaced by collapse as $N \to \infty$. For the case $\theta = 0$, the infinite N limit resembles a 3D dipolar gas with a Fermi surface deformation that can be tuned by varying the interlayer distance dk_F.

Our predicted stripe phases should be accessible in experiments on polar molecules with sufficiently large dipole moments. Even though recent experiments have demonstrated the possibility to trap atoms in uniform potentials [53], we do not expect a sufficiently slowly varying harmonic potential to affect qualitatively our results, as far as the local density approximation can be applied. One also needs to consider the issue of losses in experiments when strong interactions are involved. The restricted motion in the 2D geometry reduces the possibility of head-to-tail collisions between dipoles, which underlies the dominant loss process in dipolar gases, but such collisions are not necessarily suppressed when we have a large dipole tilt. However, we expect that chemically stable molecules such as ^{23}Na ^{40}K [18] will make it possible to probe this regime of parameter space.

In the future, it would be interesting to extend our results to finite temperature, where the proliferation of topological defects can melt the stripe phase [54]. Furthermore, one could investigate the effects of pairing using more sophisticated approaches to the multilayer system such as the Euler-Lagrange Fermi-hypernetted-chain approximation [55]. In particular, it would be intriguing to assess the fate of the stripe phase for finite N, as well as the collapse region when $N \to \infty$, by analyzing the instabilities of the "bound-state regime" where the dipoles preferentially form tightly bound chains. Finally, there is the intriguing question of how our predicted phase diagram connects with other instabilities such as nematic phases or collapse within the stripe phase. These themes clearly go beyond the scope of the present work and are left for future investigations.

ACKNOWLEDGMENTS

We are grateful to G. M. Bruun and P. A. Marchetti for useful discussions. F.M.M. acknowledges financial support from the Ministerio de Economía y Competitividad (MINECO), projects No. MAT2011-22997 and No. MAT2014-53119-C2-1-R. M.M.P. acknowledges support from the EPSRC under Grant No. EP/H00369X/2.

APPENDIX: NONINTERACTING STATIC STRUCTURE FACTOR

We start with the general expression for the noninteracting static structure factor in two dimensions [48]:

$$S^{(0)}(\mathbf{q}) = 1 - \frac{1}{n}\int \frac{d\mathbf{k}}{(2\pi)^2} n_{\mathbf{k}} n_{\mathbf{k}+\mathbf{q}}, \tag{A1}$$

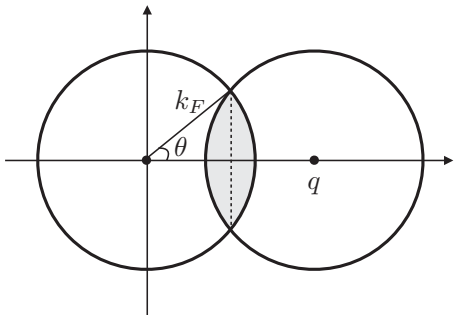

FIG. 10. Two identical circles of radius k_F, where the centers are separated by a distance q in k space. The area of the shaded overlapping region corresponds to the integral in Eq. (A1), defining the noninteracting static structure factor in 2D.

where n is the 2D density and $n_{\mathbf{k}} = \Theta(k_F - k)$ the zero-temperature Fermi distribution function. Here, the integral simply corresponds to calculating the area A of the overlap region between two identical circles of radius k_F, as shown in Fig. 10. Due to the symmetry of the problem, we only need to consider half of the overlap region as follows.

Assuming $q < 2k_F$, we first determine the segment area spanned by the angle 2θ in the left circle of Fig. 10:

$$A_{\text{seg}} = k_F^2 \theta,$$

where $\cos\theta = q/2k_F$. Next, we determine the area of the left triangle obtained by drawing a line through the points where the circles intersect:

$$A_\Delta = \frac{1}{2} k_F q \sin\theta = \frac{1}{2} k_F q \sqrt{1 - \left(\frac{q}{2k_F}\right)^2}.$$

Then we obtain:

$$\begin{aligned} A &= 2(A_{\text{seg}} - A_\Delta) \\ &= 2k_F^2 \arccos\left(\frac{q}{2k_F}\right) - k_F q \sqrt{1 - \left(\frac{q}{2k_F}\right)^2}. \end{aligned} \tag{A2}$$

Inserting (A3) into (A1), and using the fact that $\arcsin x = \pi/2 - \arccos x$, we finally recover Eq. (6) in the main text.

[1] M. A. Baranov, Phys. Rep. **464**, 71 (2008).
[2] T. Lahaye, C. Menotti, L. Santos, M. Lewenstein, and T. Pfau, Rep. Prog. Phys. **72**, 126401 (2009).
[3] M. A. Baranov, M. Dalmonte, G. Pupillo, and P. Zoller, Chem. Rev. **112**, 5012 (2012).
[4] G. Grüner, Rev. Mod. Phys. **60**, 1129 (1988).
[5] S. A. Kivelson, E. Fradkin, and V. J. Emery, Nature (London) **393**, 550 (1998).
[6] S. A. Kivelson, I. P. Bindloss, E. Fradkin, V. Oganesyan, J. M. Tranquada, A. Kapitulnik, and C. Howald, Rev. Mod. Phys. **75**, 1201 (2003).
[7] B. Naylor, A. Reigue, E. Maréchal, O. Gorceix, B. Laburthe-Tolra, and L. Vernac, Phys. Rev. A **91**, 011603 (2015).
[8] M. Lu, N. Q. Burdick, and B. L. Lev, Phys. Rev. Lett. **108**, 215301 (2012).
[9] K. Aikawa, A. Frisch, M. Mark, S. Baier, R. Grimm, and F. Ferlaino, Phys. Rev. Lett. **112**, 010404 (2014).
[10] K. Aikawa, S. Baier, A. Frisch, M. Mark, C. Ravensbergen, and F. Ferlaino, Science **345**, 1484 (2014).
[11] L. D. Carr, D. DeMille, R. V. Krems, and J. Ye, New J. Phys. **11**, 055049 (2009).

[12] K. K. Ni, S. Ospelkaus, M. H. G. De Miranda, A. Pe'er, B. Neyenhuis, J. J. Zirbel, S. Kotochigova, P. S. Julienne, D. S. Jin, and J. Ye, Science **322**, 231 (2008).
[13] S. Ospelkaus, K.-K. Ni, D. Wang, M. H. G. de Miranda, B. Neyenhuis, G. Quéméner, P. S. Julienne, J. L. Bohn, D. S. Jin, and J. Ye, Science **327**, 853 (2010).
[14] K. K. Ni, S. Ospelkaus, M. H. G. De Miranda, A. Pe'er, B. Neyenhuis, J. J. Zirbel, S. Kotochigova, P. S. Julienne, D. S. Jin, and J. Ye, Nature (London) **464**, 1324 (2010).
[15] M.-S. Heo, T. T. Wang, C. A. Christensen, T. M. Rvachov, D. A. Cotta, J.-H. Choi, Y.-R. Lee, and W. Ketterle, Phys. Rev. A **86**, 021602 (2012).
[16] M. Repp, R. Pires, J. Ulmanis, R. Heck, E. D. Kuhnle, M. Weidemüller, and E. Tiemann, Phys. Rev. A **87**, 010701 (2013).
[17] C.-H. Wu, J. W. Park, P. Ahmadi, S. Will, and M. W. Zwierlein, Phys. Rev. Lett. **109**, 085301 (2012).
[18] J. W. Park, S. A. Will, and M. W. Zwierlein, Phys. Rev. Lett. **114**, 205302 (2015).
[19] M. H. G. de Miranda, A. Chotia, B. Neyenhuis, D. Wang, G. Quéméner, S. Ospelkaus, J. L. Bohn, J. Ye, and D. S. Jin, Nat. Phys. **7**, 502 (2011).
[20] T. Miyakawa, T. Sogo, and H. Pu, Phys. Rev. A **77**, 061603 (2008).
[21] T. Sogo, L. He, T. Miyakawa, S. Yi, H. Lu, and H. Pu, New J. Phys. **11**, 055017 (2009).
[22] Y. Endo, T. Miyakawa, and T. Nikuni, Phys. Rev. A **81**, 063624 (2010).
[23] J.-N. Zhang and S. Yi, Phys. Rev. A **80**, 053614 (2009).
[24] J.-N. Zhang and S. Yi, Phys. Rev. A **81**, 033617 (2010).
[25] J. Krieg, P. Lange, L. Bartosch, and P. Kopietz, Phys. Rev. A **91**, 023612 (2015).
[26] D. Baillie, R. N. Bisset, and P. B. Blakie, Phys. Rev. A **91**, 013613 (2015).
[27] Z.-K. Lu and G. V. Shlyapnikov, Phys. Rev. A **85**, 023614 (2012).
[28] Y. Yamaguchi, T. Sogo, T. Ito, and T. Miyakawa, Phys. Rev. A **82**, 013643 (2010).
[29] K. Sun, C. Wu, and S. Das Sarma, Phys. Rev. B **82**, 075105 (2010).
[30] M. Babadi and E. Demler, Phys. Rev. B **84**, 235124 (2011).
[31] L. M. Sieberer and M. A. Baranov, Phys. Rev. A **84**, 063633 (2011).
[32] M. M. Parish and F. M. Marchetti, Phys. Rev. Lett. **108**, 145304 (2012).
[33] B. P. van Zyl, W. Kirkby, and W. Ferguson, Phys. Rev. A **92**, 023614 (2015).
[34] N. Matveeva and S. Giorgini, Phys. Rev. Lett. **109**, 200401 (2012).
[35] G. M. Bruun and E. Taylor, Phys. Rev. Lett. **101**, 245301 (2008).
[36] Z. Wu, J. K. Block, and G. M. Bruun, Phys. Rev. B **91**, 224504 (2015).
[37] J. K. Block and G. M. Bruun, Phys. Rev. B **90**, 155102 (2014).
[38] F. M. Marchetti and M. M. Parish, Phys. Rev. B **87**, 045110 (2013).
[39] K. S. Singwi, M. P. Tosi, R. H. Land, and A. Sjölander, Phys. Rev. **176**, 589 (1968).
[40] A. Pikovski, M. Klawunn, G. V. Shlyapnikov, and L. Santos, Phys. Rev. Lett. **105**, 215302 (2010).
[41] N. Matveeva and S. Giorgini, Phys. Rev. A **90**, 053620 (2014).
[42] D.-W. Wang, M. D. Lukin, and E. Demler, Phys. Rev. Lett. **97**, 180413 (2006).
[43] J. K. Block, N. T. Zinner, and G. M. Bruun, New J. Phys. **14**, 105006 (2012).
[44] U. R. Fischer, Phys. Rev. A **73**, 031602 (2006).
[45] P. Lange, J. Krieg, and P. Kopietz, Phys. Rev. A **93**, 033609 (2016).
[46] Q. Li, E. H. Hwang, and S. Das Sarma, Phys. Rev. B **82**, 235126 (2010).
[47] L. Zheng and A. H. MacDonald, Phys. Rev. B **49**, 5522 (1994).
[48] G. F. Giuliani and G. Vignale, *Quantum Theory of the Electron Liquid* (Cambridge University Press, Cambridge, UK, 2005).
[49] F. Stern, Phys. Rev. Lett. **18**, 546 (1967).
[50] A. G. Volosniev, N. T. Zinner, D. V. Fedorov, A. S. Jensen, and B. Wunsch, J. Phys. B **44**, 125301 (2011).
[51] A. Volosniev, J. Armstrong, D. Fedorov, A. Jensen, and N. Zinner, Few-Body Syst. **54**, 707 (2013).
[52] L. Świerkowski, D. Neilson, and J. Szymański, Phys. Rev. Lett. **67**, 240 (1991).
[53] A. L. Gaunt, T. F. Schmidutz, I. Gotlibovych, R. P. Smith, and Z. Hadzibabic, Phys. Rev. Lett. **110**, 200406 (2013).
[54] Z. Wu, J. K. Block, and G. M. Bruun, Sci. Rep. **6**, 19038 (2016).
[55] S. H. Abedinpour, R. Asgari, B. Tanatar, and M. Polini, Ann. Phys. **340**, 25 (2014).